AGU PUBLICATIONS

Journal of Advances in Modeling Earth Systems

RESEARCH ARTICLE
10.1002/2015MS000579

Companion to *Li et al.* [2016], doi:10.1002/2015MS000578.

Key Points:
- Summer urban land use impact are strongly affected by the precipitation amount
- Winter urban land use impacts are mostly affected by the building heating
- Future urban-natural vegetation temperature contrasts are decreasing primarily in winter

Correspondence to:
D. Li,
lidan@bu.edu

Citation:
Li, D., S. Malyshev, and E. Shevliakova (2016), Exploring historical and future urban climate in the Earth System Modeling framework: 2. Impact of urban land use over the Continental United States, *J. Adv. Model. Earth Syst.*, *8*, 936–953, doi:10.1002/2015MS000579.

Received 29 OCT 2015
Accepted 11 MAY 2016
Accepted article online 17 MAY 2016
Published online 12 JUN 2016

Exploring historical and future urban climate in the Earth System Modeling framework: 2. Impact of urban land use over the Continental United States

Dan Li[1,2], Sergey Malyshev[3], and Elena Shevliakova[4]

[1]Program of Atmospheric and Oceanic Sciences, Princeton University, Princeton, New Jersey, USA, [2]Department of Earth and Environment, Boston University, Boston, Massachusetts, USA, [3]Department of Ecology and Evolutionary Biology, Princeton University, Princeton, New Jersey, USA, [4]Geophysical Fluid Dynamics Laboratory, Princeton, New Jersey, USA

Abstract Using a newly developed urban canopy model (UCM) coupled to the Geophysical Fluid Dynamics Laboratory (GFDL) land model LM3 (LM3-UCM), this study examines the urban land use impacts over the Continental United States (CONUS) under the present-day climate and two future scenarios. Using natural (undisturbed) vegetation systems as references where no land use has occurred, the LM3-UCM simulations show that the spatial pattern of summer (June, July, and August) temperature differences between urban and natural vegetation systems is primarily controlled by the spatial pattern of differences in evapotranspiration, which further depends on the spatial distribution of precipitation. The magnitude of temperature differences generally increases as the summer precipitation amount increases and then levels off when the total summer precipitation amount exceeds 400 mm, which is broadly consistent with previous studies but with significant variability. In winter (December, January, February), the magnitude of temperature differences is more controlled by the building heating than the precipitation amount. At high latitudes where snow is an important factor in radiative balance, the magnitude is also affected by a larger net shortwave radiation input for urban areas due to the lower albedo of cities. Although both urban and natural vegetation temperatures increase as the climate warms, their increasing rates are different and hence their differences change with time. It is found that the multidecadal trend of summer temperature difference is negligible. However, the winter temperature difference shows a strong negative trend, which is caused by reduced building heating requirements under a warming climate.

1. Introduction

This is the second part of the study exploring historical and future urban climate in the Geophysical Fluid Dynamics Laboratory (GFDL) Earth System Modeling framework. Part I of the study described a new urban canopy model (UCM) coupled to the land model LM3 (hereafter LM3-UCM) and evaluated it on daily to monthly scales against observational data sets in three cities (Marseille in France, Basel in Switzerland and Baltimore in the United States). This study presents long-term, 1700–2100, regional simulations over the Continental United States (hereafter CONUS).

LM3-UCM represents subgrid scale surface heterogeneity as a collection of tiles, namely, natural (undisturbed) vegetation, pasture, cropland, urban, and secondary vegetation tiles [*Malyshev et al.*, 2015; *Milly et al.*, 2014; *Shevliakova et al.*, 2009]. Each tile has its own energy and water balances throughout the vertical column, including its own exchange with the atmosphere, while the atmosphere only feels the area-averaged fluxes. Only urban tiles are handled by the UCM. This study focuses on the canopy air temperature (T_{ca}) difference between urban canyon and natural (undisturbed) vegetation, which reflects the impacts of urban land use as compared to places where no land use has occurred. It is pointed out here that canopy air temperature is not specifically tied to urban canopies but rather a term used to distinguish from reference temperature that is often reported at 2 m above the displacement height (for more detailed discussions, see *Malyshev et al.* [2015]). Daily averaged temperature is used in our study unless specified otherwise.

The urban land use impact on temperature has been studied extensively theoretically, numerically, and experimentally at city scales and is often called the "urban heat island" effect [*Arnfield*, 2003; *Grimmond*, 2007;

Oke, 1982]. The urban heat island intensity is usually defined as the maximum difference between some representative or averaged urban and rural temperatures [*Oke*, 2006; *Stewart*, 2011]. As expected and as shown by many studies, the urban heat island intensity is highly dependent on the definitions of "urban" and "rural" [see e.g., *Grimmond et al*., 1993; *Zhou et al*., 2015]. To distinguish our study from typical observational studies on urban heat islands, we will only use the term "urban heat island effect" to refer to the difference between urban temperature and some representative or averaged rural temperature in this paper; while the main focus of this study, namely, the temperature difference between urban canyon and natural/undisturbed vegetation, will be referred to as the "urban land use impact." The similarity and difference between the "urban heat island effect" and the "urban land use impact" will be discussed.

Understanding the urban heat island effect or urban land use effect together with the climate change impact has been the subject of active research using regional climate models [*Argueso et al*., 2014, 2015; *Conlon et al*., 2016; *Georgescu*, 2015; *Georgescu et al*., 2013, 2014]. This is largely due to the high resolution of these models and the availability of urban representations in these models [*Chen et al*., 2011]. On the other hand, there are fewer studies investigating the urban heat island effect or urban land use impact at continental/global scales [*Fischer et al*., 2012; *McCarthy et al*., 2010; *Oleson*, 2012; *Oleson et al*., 2011; *Zhao et al*., 2014]. Many global modeling studies on the impacts of land use/land cover change have neglected the urban land use [*de Noblet-Ducoudre et al*., 2012; *Pitman et al*., 2009]. Recently efforts have been made to include urban representations in global climate models (GCMs) and earth system models (ESMs), including the Community Climate System Model (CCSM) [*Oleson*, 2012; *Oleson et al*., 2011] and the Hadley Center Global Climate Model (HadAM3) [*McCarthy et al*., 2010]. Using the Community Land Model (i.e., the terrestrial component of the CCSM) coupled with an urban canopy model (CLMU), *Oleson et al*. [2011] reported that when using the area-average of vegetation air temperatures at reference height as the rural reference, the urban heat island intensity averaged over all urban areas resolved in their global simulation was about 1.1^{o}C, which is nearly half of the simulated 21st mid-century warming over global land due to increasing greenhouse gases under the Intergovernmental Panel on Climate Change Fourth Assessment Report (IPCC AR4) A2 scenario. It was further reported that urban-rural contrasts of temperatures and surface energy budgets were different over different regions, which is consistent with a previous global study using HadAM3 [*McCarthy et al*., 2010]. However, the factors controlling the spatial pattern of urban-rural temperature differences were not systematically examined in these studies. A more recent study [*Zhao et al*., 2014] that focused on the spatial pattern of urban heat islands over the North America using numerical simulations and satellite observations found that the annual mean daytime urban heat island intensity was strongly correlated with the annual mean precipitation amount. They used nine urban pixels selected in the city center and 1–3 patches of 9–49 pixels (3×3 to 7×7) in the surrounding rural land to calculate urban and rural temperatures, respectively. They further attributed this strong correlation to the urban-rural contrast of so-called "convection efficiency," which is associated with the urban-rural contrast of aerodynamic resistance. However, they did not examine the seasonal variability of urban heat island intensity (e.g., summer versus winter). In addition, the role of human activities such as urban morphologies and building heating/cooling in controlling the urban heat island intensity was not explicitly addressed.

The number of modeling studies of future urban heat islands or urban land use impacts using GCMs or ESMs is even fewer [*McCarthy et al*., 2010; *Oleson*, 2012]. *McCarthy et al*. [2010] and *Oleson* [2012] both reported modest decreases in urban heat islands as the climate warms and *Oleson* [2012] further showed that the decreases were much stronger in boreal winter. On the other hand, *Fischer et al*. [2012] showed that in some regions such as the northern Europe (47–60^{o}N, 0–30^{o}E), southern Europe (36–47^{o}N, 0–30^{o}E), and northern Africa (20–36^{o}N, 0–30^{o}E), summer daily mean urban heat islands were positively correlated with daily mean temperatures, implying that the urban-rural contrast of temperature would be enhanced if the mean temperature increased in these regions. As such, how urban temperatures will evolve under a warming climate remains an elusive yet very important question for human society, since urban residents not only face health risks associated with global warming due to increasing greenhouse gases, they also experience heat stresses induced by urban land use.

As described in Part I, a new UCM (LM3-UCM) is developed within the terrestrial component of GFDL GCMs and ESMs. Given the differences between various GCMs and ESMs, and the differences between urban parameterizations, it is important to inter-compare the simulated urban climate from different GCMs and ESMs. This study is our first step toward this overarching goal in which we present the simulated urban land

use impact on temperature over the CONUS using LM3-UCM described in Part I. The LM3-UCM is forced by outputs from GFDL's Earth System Model (ESM2Mb) [*Dunne et al*., 2012a, 2012b; *Malyshev et al*., 2015] for Coupled Model Inter-comparison Project phase 5 (CMIP5) simulations. Hence the experiments presented in this paper are offline land model simulations with the atmospheric forcing (atmospheric temperature, specific humidity, wind, downward radiative fluxes, and precipitation) saved from the ESM2Mb, which do not experience any changes from the inclusion of LM3-UCM. The focus of this part is the difference between urban canyon and natural vegetation in terms of canopy air temperature and the response of this difference to climate change. Our experimental design (i.e., offline land model simulations) allows characterizing such difference without introducing urban feedbacks on climate, which can be included in the future when LM3-UCM is incorporated into the operational land model and is coupled with an atmospheric model [*Jacobson and Ten Hoeve*, 2012; *McCarthy et al*., 2010]. We acknowledge that our current approach does not allow us to study the impact of urbanization on the atmosphere, which will require a high resolution coupled climate model. However, understanding the behavior of urban tiles in an offline mode provides the basis for studying their impact in coupled simulations. We also point out that the development of high resolution atmospheric models such as the GFDL global HIgh Resolution Atmospheric Model (HiRAM) provides opportunities for conducting high resolution coupled land-atmosphere simulations in the future to explicitly study the impact of urbanization on regional climate.

2. Methodology

Using LM3-UCM, we conduct long-term simulations (from 1700 to 2100) over the large North American domain (20°N – 55°N, 130°W – 60°W), which covers the CONUS and parts of Canada and Mexico, at the resolution of 50 km, which is comparable to the spatial resolution of next-generation GCMs and ESMs. The forcing is taken from GFDL's ESM2Mb model outputs [*Dunne et al*., 2012a, 2012b; *Malyshev et al*., 2015], which has a spatial resolution of 2 by 2.5 degrees and a temporal resolution of 3 h. The first 160 years (from 1700 to 1860) are treated as the spinup period and are not analyzed here. From 2005 to 2010, the two most extreme Representative Concentration Pathways (RCP) (i.e., RCP2.6 and RCP8.5) in CMIP5 are used to represent the range of possible future climate change scenarios.

Unlike many CMIP5 land models that use fractions of land-use categories as input, LM3 uses transition rates among different land-use categories provided by *Hurtt et al*. [2011]. These transitions occur among the aforementioned five different tiles: natural vegetation, pasture, cropland, urban, and secondary vegetation. These transitions represent processes such as deforestation of natural and secondary vegetation for cropland and pasture, natural and secondary wood harvesting, abandonment of agricultural land and conversion of different lands to urban environments, which capture more comprehensively the subgrid dynamics among different land-use categories [*Malyshev et al*., 2015; *Shevliakova et al*., 2013, 2009] and are more consistent with the CMIP5 scenarios [*Hurtt et al*., 2011] than the approach using fractions of land-use categories. In particular, to represent transitions from rural land to urban land and vice versa, LM3-UCM allows a fraction of vegetation tile (i.e., natural vegetation, secondary vegetation, cropland, or pasture) to be changed to an urban tile, or a fraction of urban tile to be changed to a vegetation tile with energy, carbon and water conserved during these transitions, as explained in Part I. This enables investigations of the effects of urban expansion and urban abandonment. Annual transition rates from urban to vegetation tiles and vice versa are prescribed by *Hurtt et al*. [2011] for both historical periods and future scenarios. According to *Hurtt et al* [2011], while transitions into and from urban land may be small, transitions involving urban land still need to be included in ESMs due to the unique biogeophysical characteristics, high relevance to the human society, and significance as a source of anthropogenic emissions of urban land.

Figure 1a shows the annual transitions rates between urban and other land-use categories averaged over the simulation domain from 1700 to 2100 [*Hurtt et al*., 2011]. It is clear that the expansion of urban land (i.e., urbanization) rapidly accelerated around 1800. In the first 50 years of the 20th century, the rate of urbanization decreased due to the two world wars. Since 1950s, the pace of urbanization accelerated again substantially resulting in significant increases in the urban fraction as shown in Figure 1b. The two CMIP5 future scenarios assume drastically different population growth rates and thus urbanization rates. In RCP2.6 the size of future urban areas does not change from the present day (i.e., 2005), that is, the transition rates from and to urban lands are both zero (see also Figure 1b). In RCP8.5 urbanization continues but with a slower

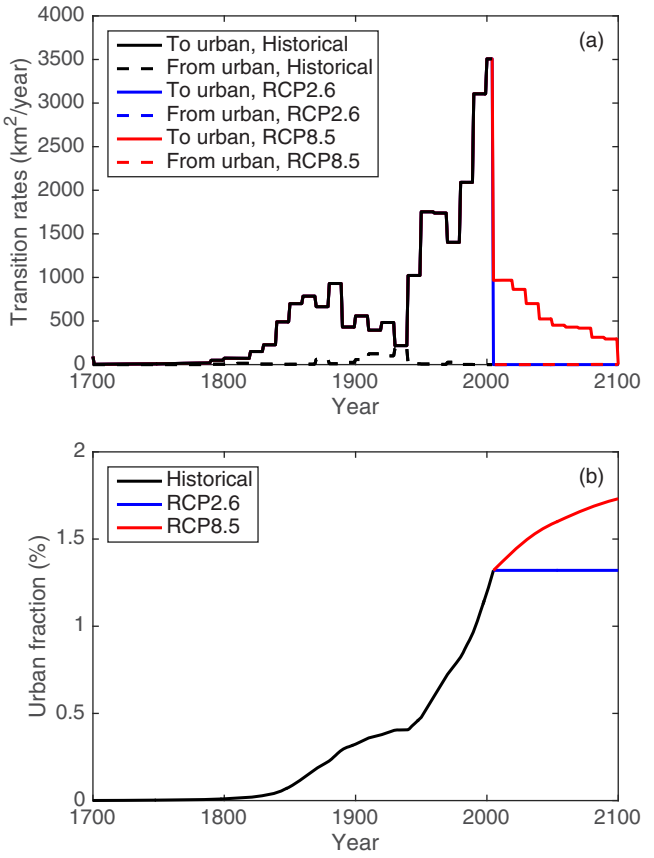

Figure 1. (a) Transition rates between urban and vegetation tiles (i.e., natural vegetation, secondary vegetation, cropland, and pasture) and (b) the urban fraction averaged over the simulation domain.

pace than during 1950–2000, that is, the transition rate to urban land is positive. The RCP8.5 assumes no decline of urban areas, that is, the transition rate from urban land to rural land is zero. Because the atmospheric forcing is prescribed in our simulations, the growth of urban areas will not have a feedback on climate. However, the growth of urban areas will still have an effect on the total urban land use impact as more and more areas in the domain will start to have urban land as time goes on.

To represent the broad geographical pattern of urban morphologies and properties, the simulation domain is subdivided into nine regions, as shown in Figure 2. Within each of these nine regions, LM3-UCM uses the same urban morphological and surface parameters, as presented in Tables 1 and 2, which also do not change with time. Most of these urban data are obtained from a unified global data set provided by *Jackson et al.* [2010]. The road substrate depth, the roughness lengths and water-holding capacities of roof and impervious ground are not available in *Jackson et al.* [2010] and are adopted from the modeling set up used in Part I. One interesting feature to point out is that the minimum and maximum building temperatures are different for some regions (see Table 2). In particular, there is almost no restriction for the minimum and maximum building temperature in region 8 (Mexico) and region 9 (Cuba), which reflects the lack of heating (in winter) and air conditioning (in summer) in these regions.

The data set developed by *Jackson et al.* [2010], which was designed for CLMU, includes morphologies and properties for three different urban tiles in each region, namely, tall building district, high density, and medium density. The parameters in Tables 1 and 2 are for the medium density urban tile, as it has the largest fraction across the domain. Note the original data set included an additional urban tile, which is low density, but it was concluded that low density urban was better modeled as a vegetated/soil surface given its low impervious fraction so it was excluded from the original data set [*Jackson et al.*, 2010; *Oleson et al.*, 2011]. In general LM3-UCM allows multiple urban tiles with different morphologies and properties to co-exist in the same grid cell (e.g., to represent the difference between high density and low density urban land). This however requires knowing transitions among these different urban tiles, which are unavailable in the land-use transition data set

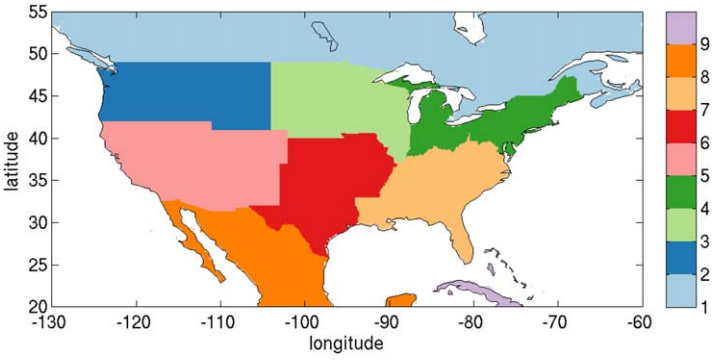

Figure 2. Nine different regions in the simulation domain. These nine different regions have different urban morphological and surface parameters, as shown in Tables 1 and 2.

Table 1. Urban Morphological Parameters for Different Regions[a]

Region Index	1	2	3	4	5	6	7	8	9
Canyon aspect ratio H/R_d	0.60	0.48	0.48	0.68	0.48	0.48	0.48	1.60	0.52
Roof fraction $R_f/(R_f+R_d)$	0.55	0.45	0.35	0.45	0.55	0.50	0.55	0.45	0.55
Vegetated ground fraction f_p	0.667	0.636	0.692	0.545	0.556	0.500	0.667	0.545	0.667
Building height H (m)	15	12	12	17	12	12	12	12	13
Roof substrate depth (m)	0.148	0.150	0.189	0.158	0.150	0.146	0.148	0.025	0.092
Wall substrate depth (m)	0.283	0.281	0.306	0.328	0.293	0.257	0.281	0.283	0.240
Road substrate depth (m)	0.5	0.5	0.5	0.5	0.5	0.5	0.5	0.5	0.5

[a]"Road" corresponds to the impervious ground in the LM3-UCM.

[*Hurtt et al*., 2011]. As a compromise, it is assumed in this study that only one urban tile is allowed in each grid cell, which is the dominant urban tile in this grid cell defined by *Jackson et al*. [2010]. Within our simulation domain, over 96% of the grid cells that have urban tiles are dominated by medium density and hence the parameters for the medium density urban tile are presented in Tables 1 and 2.

To further understand the role of urban morphologies and properties in controlling the temperature difference between urban canyon and natural vegetation, an additional simulation is conducted in which the urban morphological and surface parameters are set to be uniform across the simulation domain. These parameters were taken from the industrial/commercial urban category in the Weather Research and Forecasting Model [*Chen et al*., 2011] to present a different urban land use scenario from a different data set.

3. Results

3.1. Spatial Distribution of Urban Land Use Impacts

Figure 3 shows the simulated summer (June, July, and August, hereafter JJA) urban-natural vegetation temperature difference in the same grid cell averaged every two decades from 1881 to 2000. Any grid cell that does not have an urban tile or a natural vegetation tile is left blank in Figure 3, while any grid cell that has both an urban tile and a natural vegetation tile is color-shaded (independently of urban tile size). Since most grid cells have natural vegetation tiles, Figure 3 illustrates that the number of grid cells containing urban tiles has increased from 1881 to 2000, which is consistent with Figure 1.

The urban-natural vegetation temperature difference shows a strong spatial variability. Nonetheless, it does not change much with time on decadal time scales (see different plots of Figure 3). Figure 3 also shows that in most places the difference is positive, which is consistent with previous studies using HadAM3 [*McCarthy*

Table 2. Urban Surface Properties for Different Regions[a]

Region Index	1	2	3	4	5	6	7	8	9
Roof emissivity	0.649	0.646	0.475	0.546	0.646	0.912	0.649	0.592	0.910
Wall emissivity	0.885	0.906	0.891	0.906	0.906	0.906	0.906	0.906	0.912
Road emissivity	0.910	0.910	0.910	0.910	0.910	0.910	0.910	0.950	0.910
Roof albedo	0.277	0.304	0.370	0.316	0.304	0.178	0.277	0.206	0.290
Wall albedo	0.296	0.344	0.281	0.272	0.377	0.368	0.344	0.272	0.645
Road albedo	0.130	0.130	0.130	0.130	0.130	0.130	0.130	0.080	0.130
Roof thermal conductivity (W m^{-1} K^{-1})	0.839	0.837	1.296	1.079	0.837	0.114	0.839	27.501	0.106
Wall thermal conductivity (W m^{-1} K^{-1})	1.059	1.056	1.162	1.193	1.090	0.963	1.056	0.909	1.100
Road thermal conductivity (W m^{-1} K^{-1})	1.670	1.670	1.670	1.670	1.670	1.670	1.670	0.360	0.640
Roof heat capacity (10^6 J m^{-3} K^{-1})	0.761	0.756	0.594	0.717	0.756	0.759	0.761	1.868	0.719
Wall heat capacity (10^6 J m^{-3} K^{-1})	0.840	0.812	0.875	0.947	0.860	0.765	0.812	0.939	0.783
Road heat capacity (10^6 J m^{-3} K^{-1})	2.061	2.061	2.061	2.061	2.061	2.061	2.061	1.546	1.787
Minimum building temperature (K)	290	290	290	290	290	290	290	278	278
Maximum building temperature (K)	310	380	310	310	305	300	300	380	380
Roof water holding depth (cm)	2	2	2	2	2	2	2	2	2
Road water holding depth (cm)	1	1	1	1	1	1	1	1	1
Roof momentum roughness length (m)	0.10	0.10	0.10	0.10	0.10	0.10	0.10	0.10	0.10
Road momentum roughness length (m)	0.01	0.01	0.01	0.01	0.01	0.01	0.01	0.01	0.01

[a]"Road" corresponds to the impervious ground in the LM3-UCM.

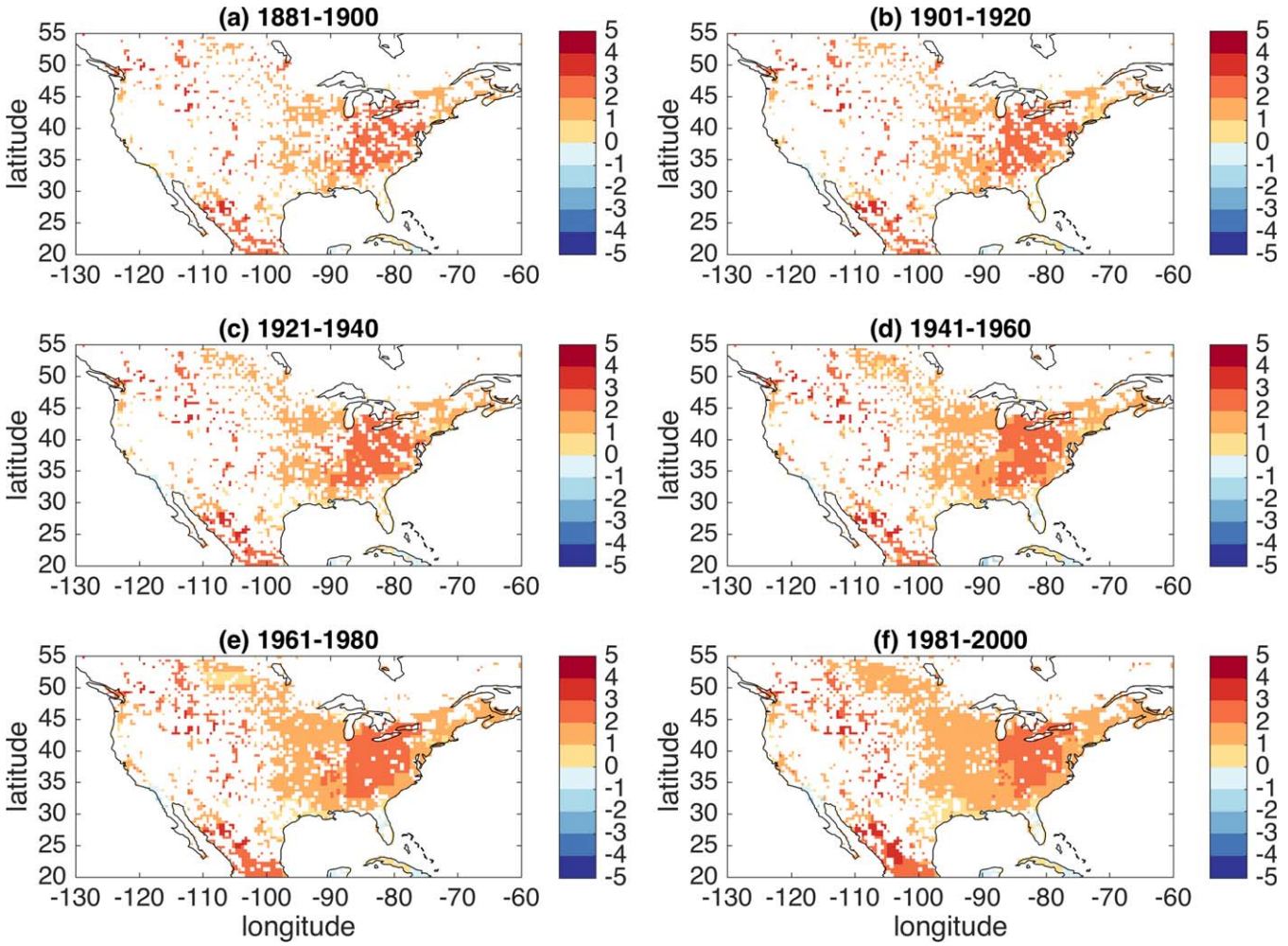

Figure 3. The simulated canopy air temperature difference between urban canyon and natural vegetation in the same grid cell in JJA averaged from (a) 1881 to 1900, (b) 1901 to 1920, (c) 1921 to 1940, (d) 1941 to 1960, (e) 1961 to 1980, and (f) 1981 to 2000. The unit is °C.

et al., 2010] and CCSM [*Oleson et al*., 2011] but using different definitions of urban and/or rural temperatures. However, some features of the spatial pattern differ from the previous two studies. In our study, the temperature differences are stronger in the eastern and western US than in the central US. In contrast, the study by *McCarthy et al*. [2010] shows a decreasing trend from the west to the east. Our simulations (see Figure 3) in general show large, positive values over the western US, extending from Canada to Mexico. This pattern has been previously shown by *McCarthy et al*. [2010] but not in the study by *Oleson et al*. [2011]. There are several possible explanations for these differences. First is the coarse model resolution used in the previous two studies due to their focus on the global picture and their use of coupled simulations. Second, canopy air temperature is used in our study while 2 m reference temperature is used by *McCarthy et al*. [2010]. The difference between canopy air temperature and reference temperature has been discussed in a recent study by *Malyshev et al*. [2015]. The study by *Oleson et al*. [2011] used air temperature in the urban canopy layer which, as mentioned in Part I, interacts with both roof and canyon, while in LM3-UCM roof and canyon have different canopy air temperatures and in this study the canyon one is used. The study by *Oleson et al*. [2011] also used reference height air temperature for rural areas. Third, our study uses natural vegetation to represent rural conditions, while the previous two studies used either the temperature of the dominant nonurban tile [*McCarthy et al*., 2010] or the area-averaged temperature of all vegetation tiles [*Oleson et al*., 2011] to represent the rural temperature. Last but not least, different urban models have different biases in the simulated urban temperatures. As shown in Part I, the canopy air temperature in the urban canyon tends to be overestimated by LM3-UCM (and also other UCMs), which could lead to an overestimation of the urban land use effect.

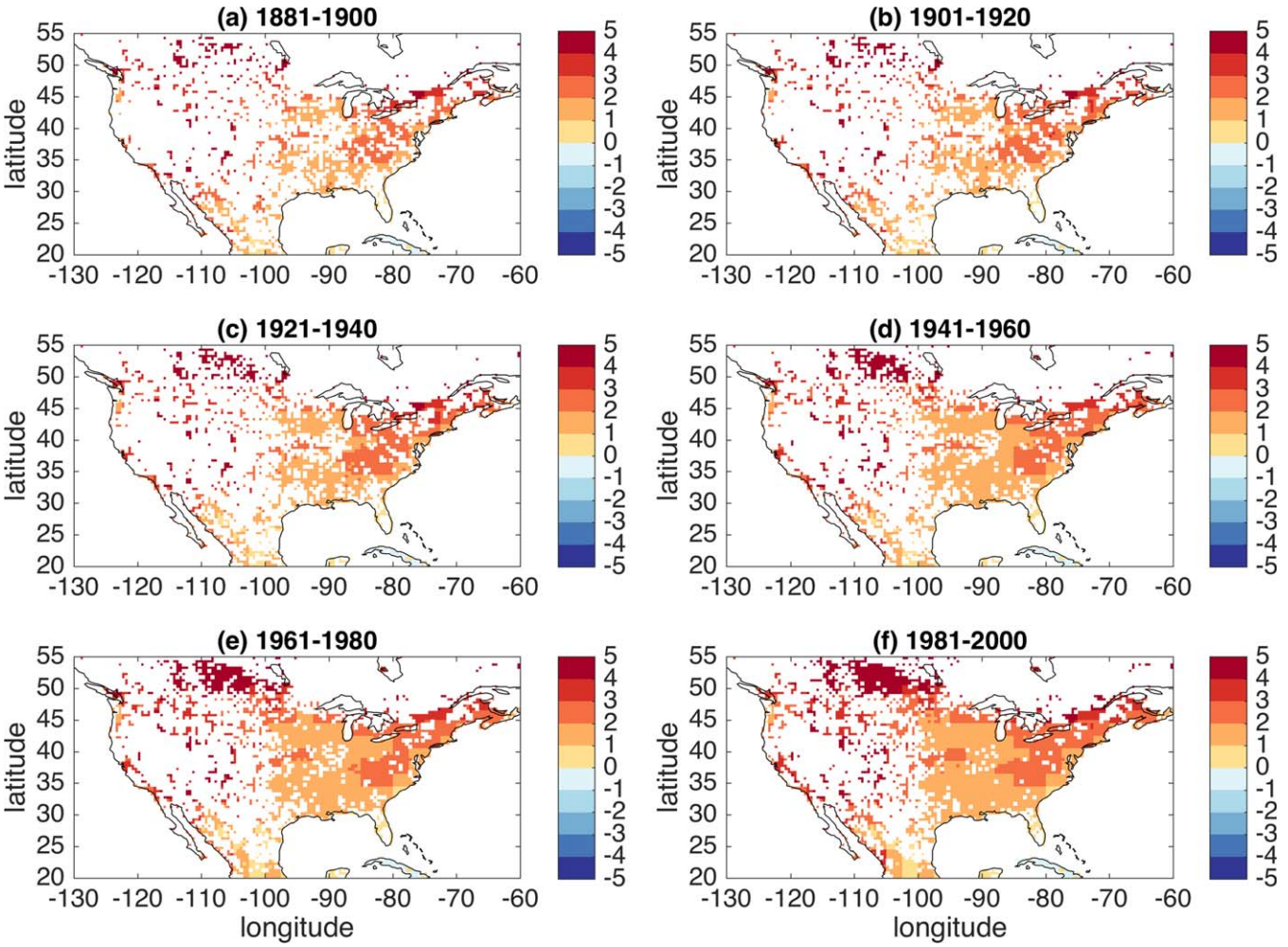

Figure 4. Similar to Figure 3 but for DJF. The unit is °C.

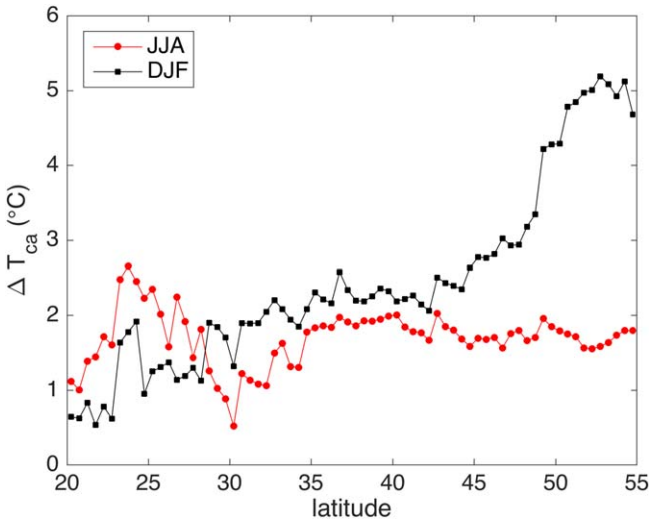

Figure 5. The zonally averaged temperature differences during 1981–2000.

Similarly, Figure 4 shows the simulated winter (December, January, and February, hereafter DJF) temperature differences (20 year-averages) throughout 1881–2000. The simulated winter temperature differences are positive in all grid cells and also show strong spatial variability. The temperature differences are strongest in the western US, followed by the eastern US and by the central US. Figure 5 further presents the zonal averages during 1981–2000. The summer (JJA) zonal average has little dependence on latitude above 30°N (i.e., excluding Mexico, Cuba and the state of Florida). In contrast, the winter (DJF) zonal average displays a strongly increasing trend northward,

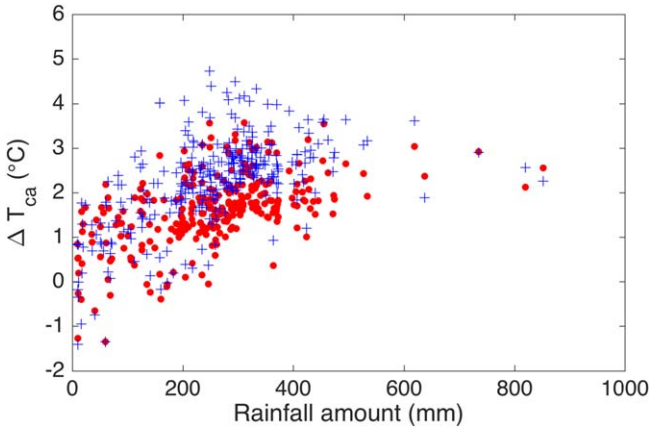

Figure 6. The relation between urban-natural vegetation temperature difference and the total rainfall amount in JJA. Red dots are simulated results using urban properties specified in Tables 1 and 2 (i.e., the urban properties are not uniform across the domain). Blue pluses are simulated results using uniform urban properties across the domain.

which, as we will show later, is likely due to higher winter building heating rates at higher latitudes.

As mentioned earlier, a recent study analyzed the spatial variability of annual mean surface urban heat islands (i.e., the surface radiative temperature was used to define the urban heat island effect) over North America and found strong contributions of local background climate (represented by the annual mean precipitation amount) to annual mean daytime urban heat islands [*Zhao et al*., 2014]. However, they did not investigate the spatial variability at seasonal time scales and they also did not examine the role of human activities such as building heating/cooling. Using our LM3-UCM simulations, we first examine the relation between summertime precipitation amount and summertime temperature differences. The spatial correlation between summertime temperature differences and the summertime precipitation amount is 0.55, higher than those with any other climatic variables, which implies that the summertime temperature differences are strongly modulated by the background climate (particularly precipitation) and is consistent with the annual mean results presented in *Zhao et al*. [2014]. Figure 6 shows that summertime temperature differences increase with the total summer precipitation amount and then level off when the total summer precipitation amount exceeds about 400 mm (see the red dots in Figure 6). The initial increase (i.e., when the total summer precipitation amount is less than 400 mm) is because water available for evapotranspiration increases with precipitation up to soil's water-holding capacity, which is higher in vegetated areas than in urban areas where a certain fraction of ground is impermeable (see Table 2). Consequently, as precipitation increases rural areas store more water and evaporate more, which concomitantly leads to a larger reduction in the vegetation temperature and amplifies the temperature difference. The "leveling" of such relationship above 400 mm, which was not observed in the study of *Zhao et al*. [2014], indicates that increasing rainfall amount no longer enhances the temperature difference, because the temperature difference is no longer controlled by water availability under such conditions (i.e., water is already sufficient for evaporation) but more by the energy availability, which is similar to the Budyko curve concept [*Budyko*, 1963].

It should be pointed out that the temperature differences shown on Figure 6 are averages for the same precipitation amount given the coarser resolution of the forcing data (2 $\times$ 2.5 degrees) than the resolution of the simulation (50 km). It can be seen from Figure 6 that there is still large variability even when the summer precipitation amounts are similar, suggesting that other factors also modulate the summer temperature difference. For example, in extremely dry areas where precipitation is minimal, the urban-rural contrast of albedo might play an important role in controlling the temperature difference. Cities can have higher or lower albedo values than rural areas, particularly considering that the effective albedo of an urban canyon is related to the height of buildings, the geometry of canyon, and the albedo values of wall and ground surfaces (see Part I).

To further understand the role of urban morphologies and properties, an additional simulation is conducted in which the urban morphological and surface parameters are set to be uniform and represent industrial/commercial urban characteristics across the simulation domain (the blue pluses in Figure 6). This additional experiment demonstrates that the summertime temperature difference-precipitation amount relation remains similar (cf. red dots and blue pluses in Figure 6) but the magnitude of temperature difference is mostly enhanced by changing the properties to represent industrial/commercial urban characteristics. The mean increase averaged over the domain is 0.6°C, suggesting an important role of urban morphologies and characteristics in controlling the summertime temperature difference.

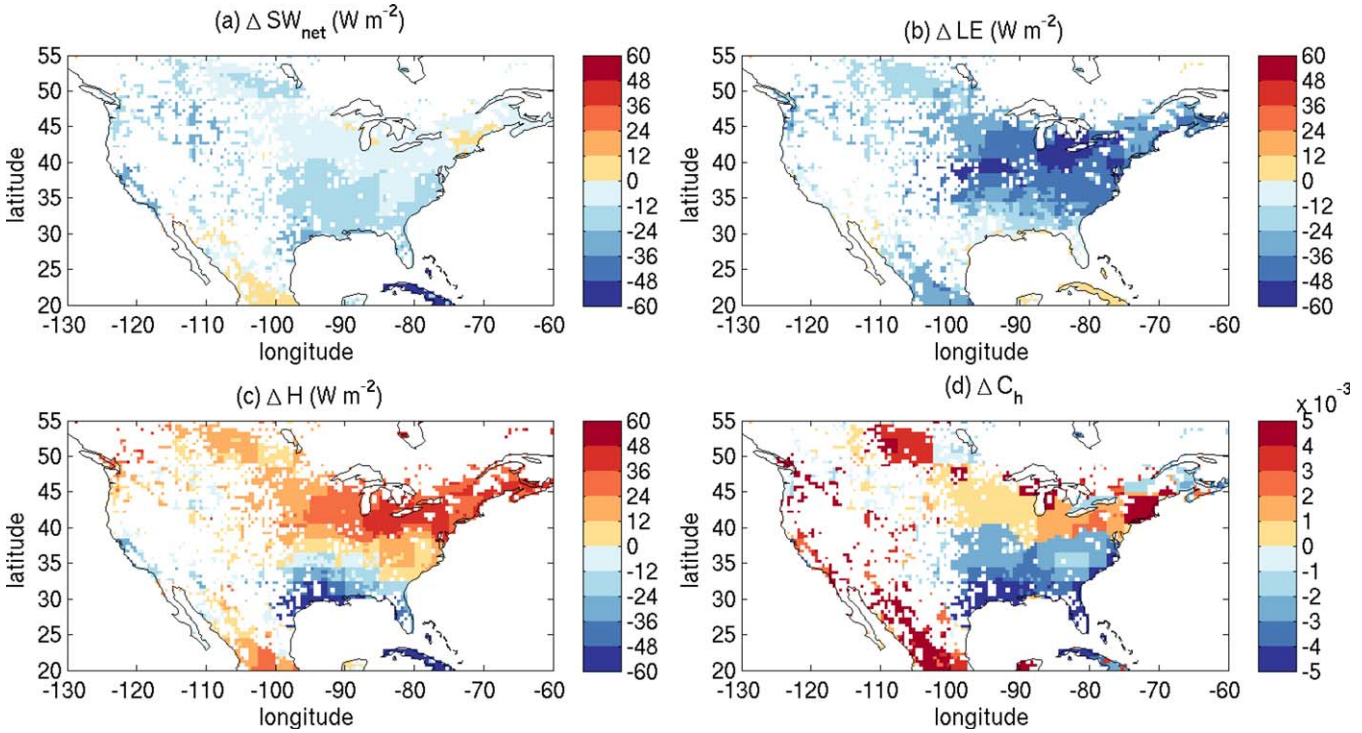

Figure 7. Differences between urban canyon and natural vegetation in JJA in terms of (a) net shortwave radiation, (b) latent heat flux, (c) sensible heat flux, (d) turbulent transfer coefficient. The results are averaged from 1981 to 2000.

In addition to the precipitation amount, the impacts of other climatic variables on summertime temperature difference are also examined. Figure 7 shows summer (JJA) urban-natural vegetation contrasts in net shortwave radiation (Figure 7a), latent heat flux (Figure 7b), sensible heat flux (Figure 7c), and turbulent transfer

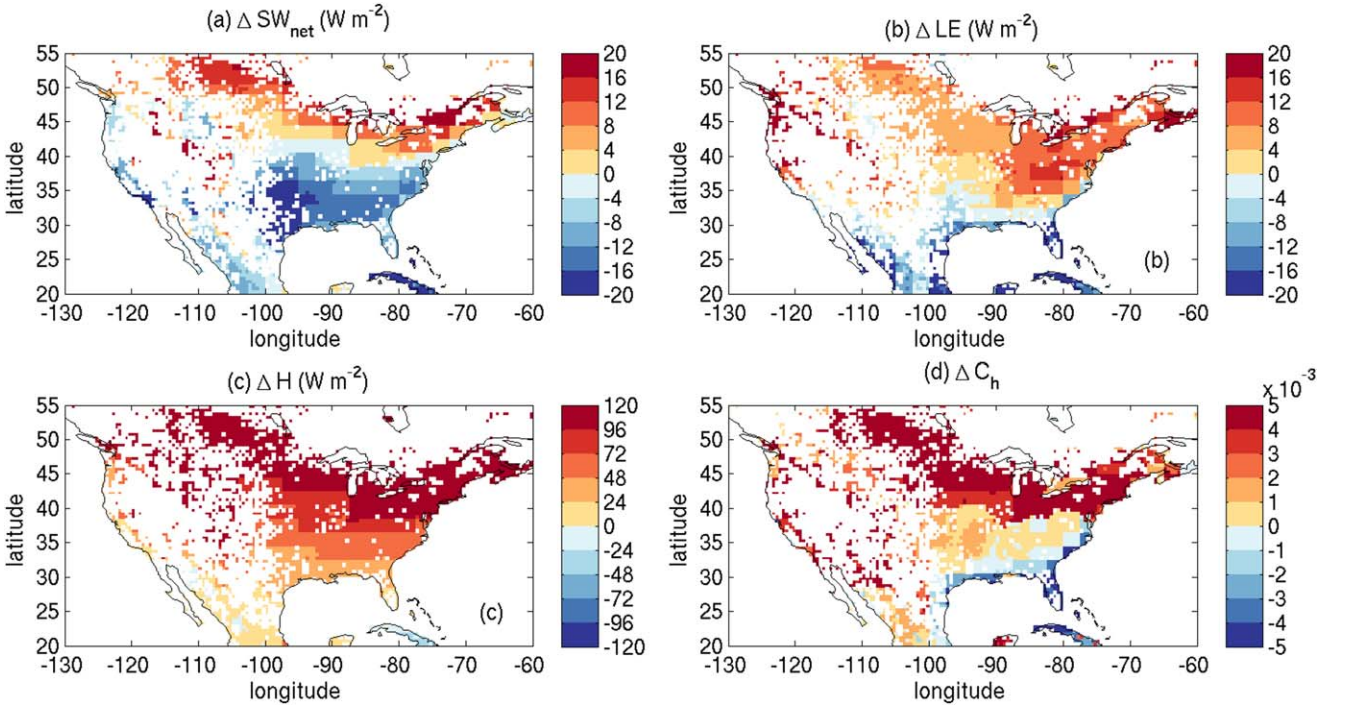

Figure 8. Similar to Figure 7 but for DJF.

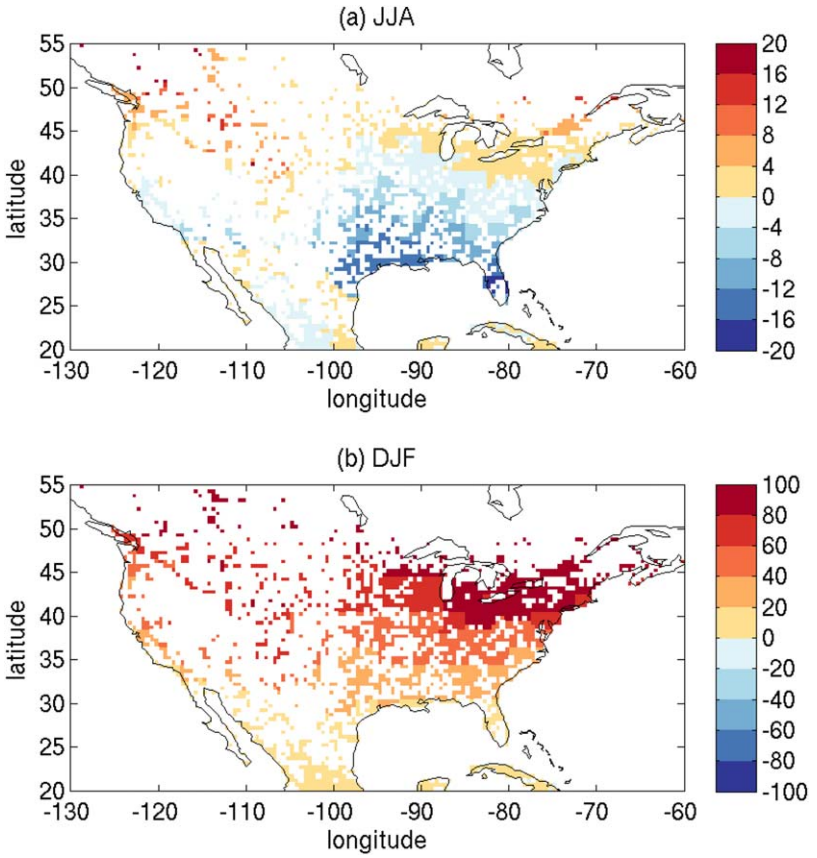

Figure 9. The heat flux (unit: W m^{-2}) into buildings from the urban canyon (i.e., through the walls, W m^{-2} of urban area) in (a) JJA and (b) DJF. Positive values denote fluxes from buildings to the urban canyon while negative values denote fluxes into buildings from the urban canyon. The results are averaged from 1981 to 2000.

coefficient (Figure 7d). There are a few important features on Figure 7 that should be mentioned here. First, the spatial correlation between temperature difference and net shortwave radiation difference is 0.3, implying that summertime temperature difference is affected but not determined by the difference in the net absorbed shortwave radiation. Second, the spatial pattern of temperature difference is slightly more correlated with the spatial pattern of latent heat flux (i.e., evapotranspiration) contrast than that of sensible heat flux contrast. The correlation between temperature difference and latent heat flux contrast is -0.47 while the correlation between temperature difference and sensible heat flux contrast is 0.42. A strong correlation between temperature difference and latent heat flux contrast suggests that the available water for evaporation plays an important role in controlling the summer temperature difference, which is consistent with the results shown in Figure 6 as well as the results shown in Part I (e.g., Marseille simulations over a dry-down period are sensitive to the initial soil moisture). Third, the spatial pattern of sensible heat flux contrast (Figure 7c) is not identical to the spatial pattern of temperature difference (Figure 3f). To understand the relation between them, we need to also consider the spatial pattern of turbulent transfer coefficient difference. The sensible heat flux H (W m^{-2}) is linked to the canopy air temperature T_{ca} (K) through $H = \rho c_p C_h U(T_{ca} - T_a)$ where ρ is the air density (kg m^{-3}), c_p is the specific heat of air under constant pressure (J kg^{-1}), C_h is the turbulent transfer coefficient for heat, U is the wind speed from the atmospheric model (m s^{-1}), T_a is the air temperature from the atmospheric model (K). The urban-natural vegetation contrast of sensible heat flux is defined as $\Delta H = \rho c_p \Delta C_h (T_{ca} - T_a) + \rho c_p C_h \Delta T_{ca}$, where Δ represents the urban-natural vegetation contrast. Note that the wind speed and the air temperature of the atmospheric layer are identical for the all subgrid tiles. As shown in Figure 7d, in the southeastern US where the temperature differences are positive ($\Delta T_{ca} > 0$), the contrasts of sensible heat flux are negative ($\Delta H < 0$) due to the negative contrasts of turbulent transfer coefficient ($\Delta C_h < 0$). This is consistent with the study by *Zhao et al.* [2014]. However, the correlation between temperature differences and the turbulent transfer coefficient differences over the whole

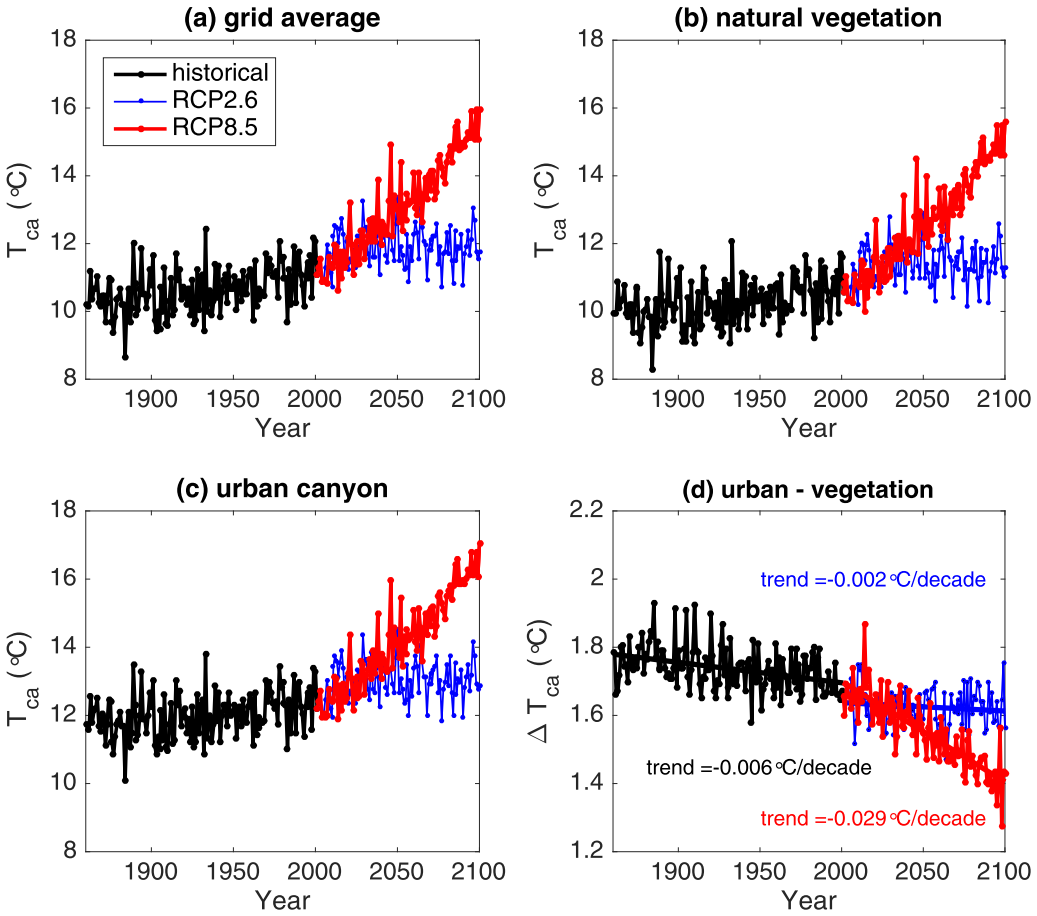

Figure 10. Simulated annual (a) grid-averaged canopy air temperature, (b) natural vegetation canopy air temperatures, (c) urban canyon canopy air temperatures, (d) the difference from 1861 to 2100. The results are area-averaged over the simulation domain.

domain is only 0.15, implying that the turbulent transfer coefficient contrast is only important regionally (e.g., over the southeastern US).

Another striking feature of Figure 7 is that different regions (defined in Figure 2) show visible boundaries in all plots. For example, the boundary between region 4 and region 7 is clearly seen in Figure 7a, which is related to differences in the building height, canyon aspect ratio and the wall albedo since these affect the effective albedo of an urban canyon (see Part I). This boundary is also visible in Figure 7d since the contrast of turbulent transfer coefficient is largely due to the difference of roughness length, and the roughness length of an urban canyon is directly related to the building height (see Part I). The negative contrasts of turbulent transfer coefficient ($\Delta C_h < 0$) in region 7 are related to the relatively lower building height in this region (e.g., compared to region 4). It is noted here that these regions are defined rather arbitrarily [*Jackson et al.*, 2010] and the boundaries seen here might not reflect the real differences in terms of urban morphologies and properties. However, these results do highlight the important role of urban morphologies and properties in modulating summertime temperature differences between urban canyon and natural vegetation, which is consistent with the results in Figure 6. They also underscore the importance of developing more accurate input data sets for large-scale and long-term urban simulations. It is also pointed out that the structures in these figures (e.g., Figures 3, 4, and 7) are finer than the resolution of nine regions in Figure 2 due to the resolution of the atmospheric forcing data, which is 2×2.5 degrees.

Similar analyses are conducted for the winter season (DJF). Figure 8 examines the contrasts of net shortwave radiation (Figure 8a), latent heat flux (Figure 8b), sensible heat flux (Figure 8c), and turbulent transfer coefficient (Figure 8d) in winter between urban canyon and natural vegetation. The large and positive contrasts of net shortwave radiation in the northern latitudes of the domain are primarily due to the snow

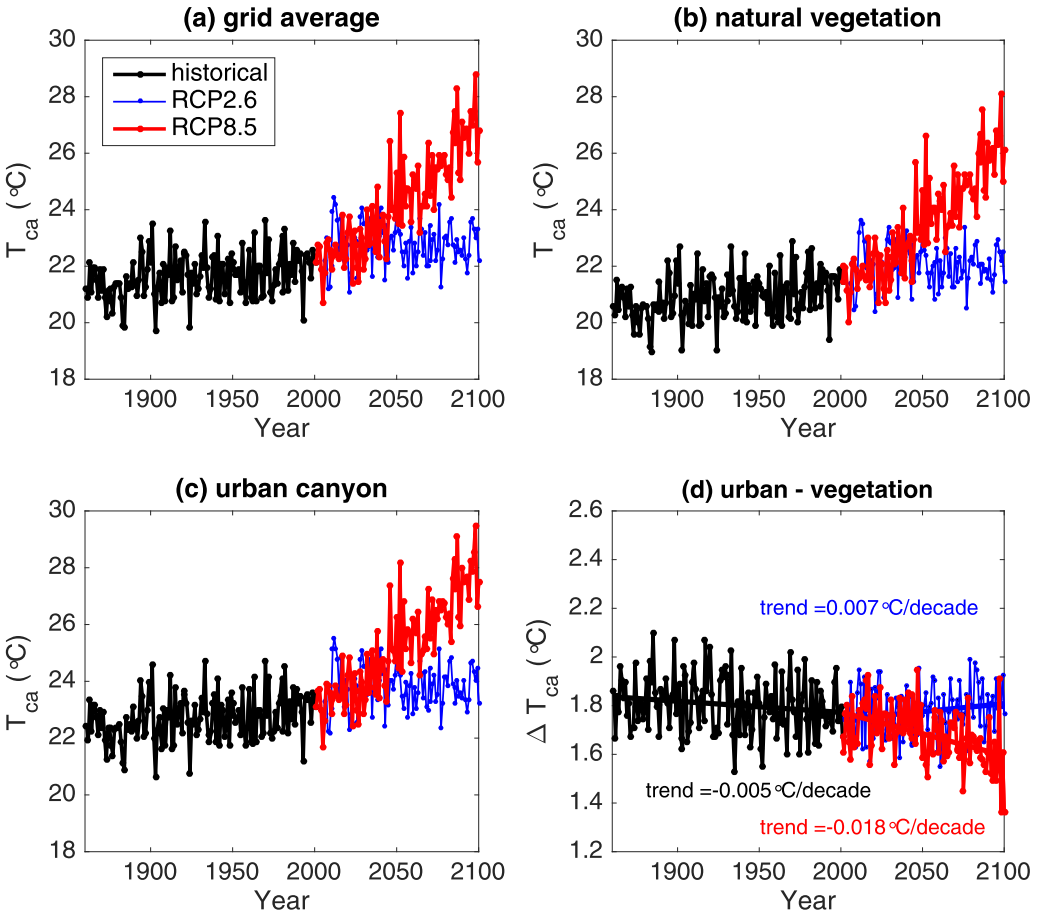

Figure 11. Similar to Figure 10 but for JJA.

cover that increases the effective albedo of vegetated land and hence reduces its net shortwave radiation. Note in the urban canyon, snow on the impervious ground becomes runoff immediately as explained in Part I so the albedo of impervious ground is effectively not affected by snow. The spatial correlations between temperature difference and net shortwave radiation, sensible heat flux, latent heat flux, and turbulent transfer coefficient contrasts are 0.68, 0.72, – 0.27, 0.64, respectively. The contrast of sensible heat flux has the highest spatial correlation with the temperature difference (also c.f. Figure 8c and Figure 4f), followed by the contrast of net shortwave radiation, while the contrast of latent heat flux has the lowest correlation. The relation between the precipitation amount and temperature difference in the winter is also examined. In contrast to the situation in summer as shown in Figure 6, the wintertime temperature difference is found not to be affected by the wintertime precipitation amount. This suggests that the strong correlation between annual mean precipitation amount and urban heat island intensities shown in *Zhao et al.* [2014] is primarily due to the high correlation in summer (as shown in our Figure 6) but not in winter. The spatial pattern of turbulent transfer coefficient difference also resembles that of temperature difference, which is surprising at first since the spatial pattern of temperature difference should be negatively correlated with the spatial pattern of turbulent transfer coefficient difference if the sensible heat flux was the same (i.e., a larger/positive urban-rural contrast of turbulent transfer coefficient should lead to a smaller/negative UHI effect if the urban-rural contrast of sensible heat flux was zero, as suggested by $\Delta H = 0 = \rho c_p \Delta C_h (T_{ca} - T_a) + \rho c_p C_h \Delta T_{ca}$). The positive correlation between temperature difference and turbulent transfer coefficient difference further underscores the importance of ΔH, which is nonzero.

The importance of ΔH in controlling winter temperature difference further suggests a critical role of building heating because in our simulations the building interior temperature is restricted to be between the maximum and minimum building temperatures specified in Table 2. Figure 9 shows the heat flux from the building interior to the wall surface per unit urban canyon area in summer (Figure 9a) and winter

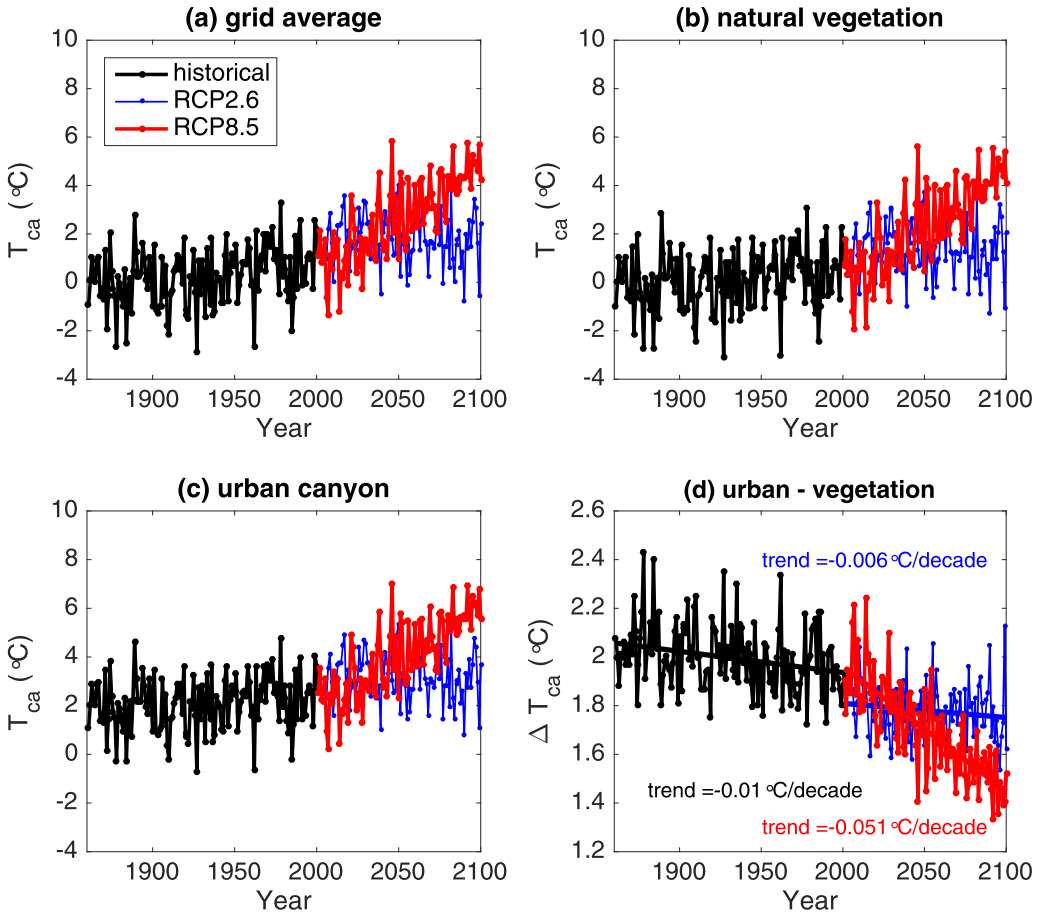

Figure 12. Similar to Figure 10 but for DJF.

(Figure 9b). These results show that the magnitude of building heat flux is much larger in winter than in summer, suggesting that building heating plays an important role in winter. In summer, the heat flux on average goes into the building interior at low latitudes but comes from the building interior at high latitudes. In winter, the heat flux is always coming from the building interior, implying that all regions require heating for buildings (i.e., input of energy). The heating maintains the building interior temperature and thus enhances the canopy air temperature of the urban canyon and concomitantly the sensible heat flux, which is the main mechanism controlling winter temperature difference between urban canyon and natural vegetation. The fact that the wintertime temperature difference is strongly controlled by building heating suggests that human behaviors play a dominant role in modulating urban land use impact on temperature in winter.

Note that our simulated summer temperature difference might be underestimated. As shown in Figure 9a, in summer the heat flux goes into the building at low latitudes. After the heat flux enters the building, it is lost in our current simulation, which cools the urban area as a whole. However, in reality the temperature of building interiors is maintained by air conditioning system, which redistributes the heat flux entering buildings back to the urban canyon and generates waste heat. This would contribute a positive amount of energy to the surface balance and warm the outside urban environment. As a result of neglecting these effects, our simulation (similar to many other UCMs) might underestimate the magnitude of summer temperature difference and their response to future climate change. However, given the relatively small magnitude of this heat flux, our conclusions should be still qualitatively correct. Future improvement of the UCM considering the effect of air conditioning is needed.

3.2. Temporal Variability of Urban Land Use Impacts

Here we investigate the long-term trends and temporal variability of urban land use impact from 1861 to 2100. Figure 10 shows the simulated annual grid-averaged (Figure 10a), natural vegetation (Figure 10b),

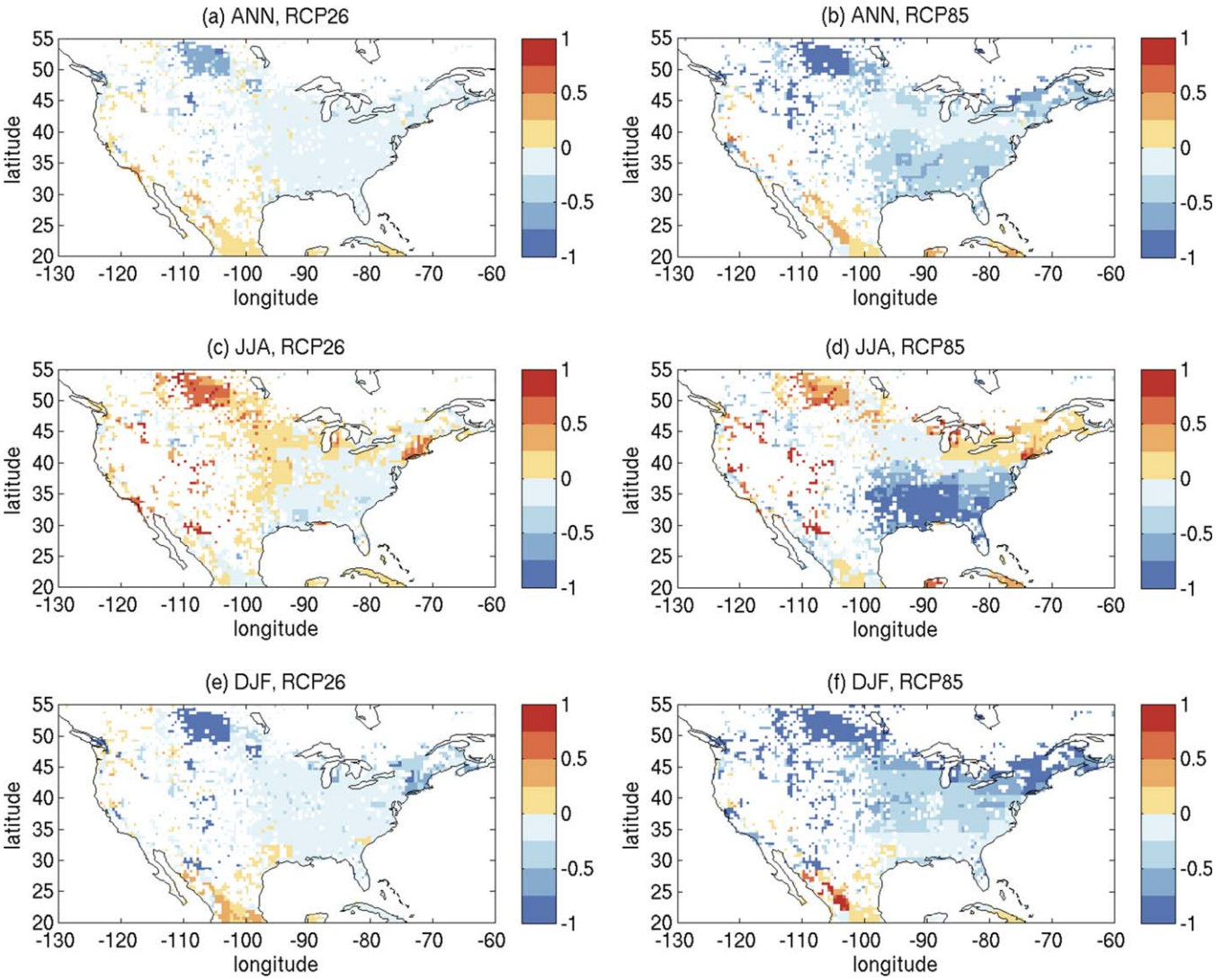

Figure 13. Contrasts between the urban-natural vegetation temperature differences in 2081–2100 and those in 1981–2000. The unit is °C.

and urban canyon (Figure 10c) canopy air temperatures, as well as the differences between urban canyon and natural vegetation canopy air temperatures (Figure 10d). The results are spatially averaged over the entire simulation domain using grid-cell areas as weights. The simulated results clearly indicate that both urban and natural vegetation's canopy air temperatures show increasing trends consistent with warming atmospheric temperatures from ESM2Mb forcing. As expected, the canopy air temperatures of subgrid tiles have larger increasing trends under scenario RCP8.5 than under RCP2.6. Our simulations further suggest that the temperature difference in the historical period and in the future decreases with warming. As Figure 10d shows, the decreasing trend was 0.006°C/decade from 1861 to present day, which is reduced to 0.002°C/decade under scenario RCP2.6 but is increased to 0.029°C/decade under scenario RCP8.5. These results are in qualitative agreement with a previous study [*Oleson*, 2012] based on coupled global simulations with the CCSM.

Similar to Figure 10, Figures 11–12 show results in JJA and DJF, respectively. These figures show that, despite the increasing trends of both urban canyon and natural vegetation canopy air temperatures, their differences decrease in both JJA and DJF. The decreasing trend is more prominent in the winter season, which is also consistent with the study by Oleson [2012]. The main cause of decreasing trend is reduced winter heating demand for buildings under a warming climate, especially at high latitudes (not shown), since building heat has been identified as a primary controlling factor for winter temperature difference

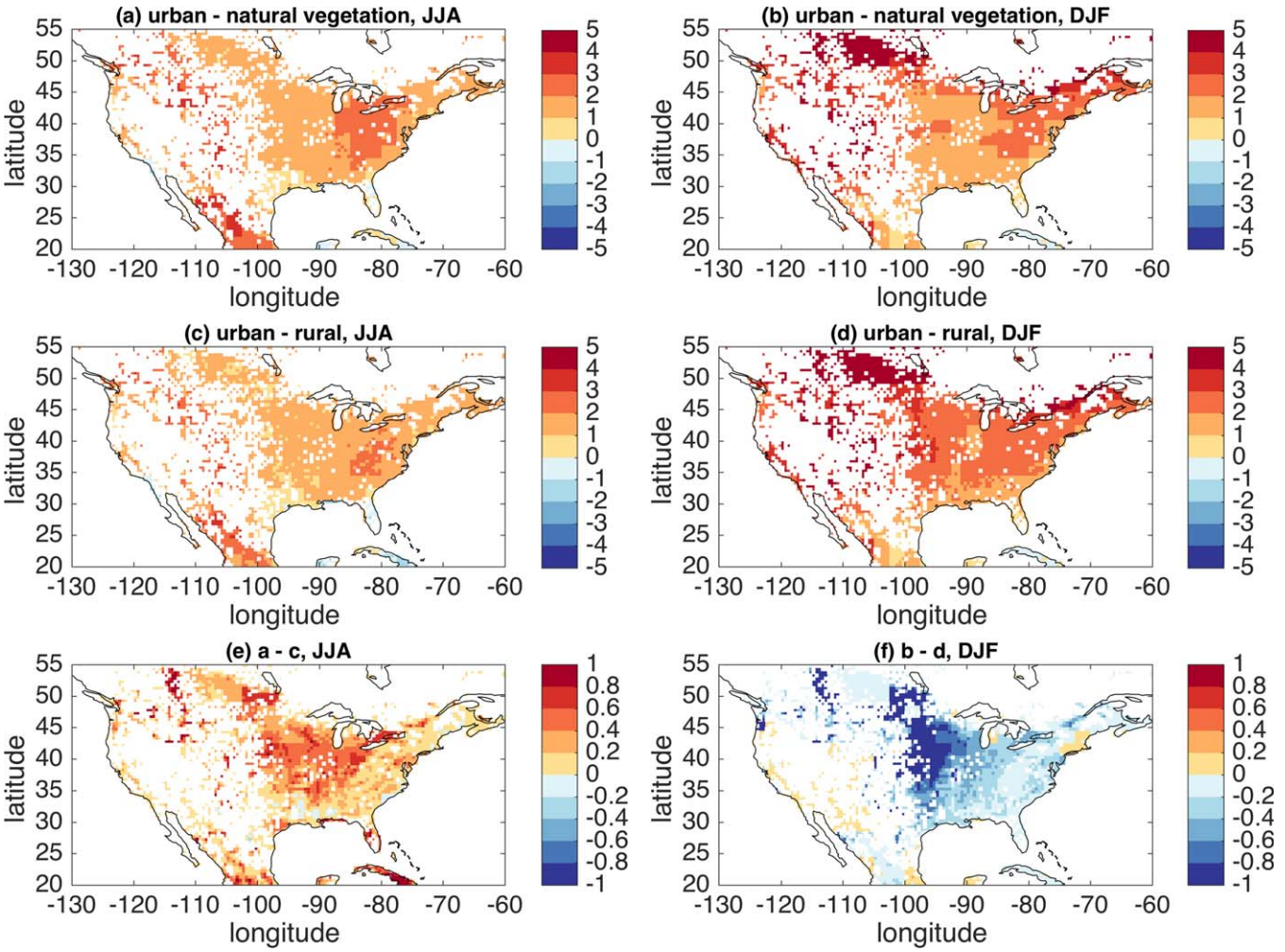

Figure 14. (a, b) The urban-natural vegetation temperature differences and (c, d) the urban-rural temperature differences and (e, f) their contrasts in (a, c, e) summer and(b, d, f) winter averaged over 1981–2000. The rural temperature in Figures 14c and 14d is an area-average of nonurban temperatures. The unit is °C.

(see Figure 9). Mann-Kendall test for detecting linear trends is used to compute the significance of these trends. All the trends shown here, except the annual and JJA trends in RCP26, are statistically significant at the 0.05 level. Note that the decreasing trends are stronger in our study than in the study by Oleson [2012] for the North America region, which can be attributed to differences in the urban model itself, the choice of rural reference, and the climate forcing trends and variability (i.e., CESM versus GFDL ESM2Mb). This calls for an intercomparison of urban simulations embedded in global climate change simulations across different models such as those proposed for the Sixth Coupled Model Intercomparison Project [*Lawrence et al*., 2016].

Figure 13 shows the contrast between urban-natural vegetation temperature difference in 2081–2100 and its counterpart in 1981–2000. The results indicate that differences in winter (Figures 13e and 13f) are more negative than the annual (Figures 13a and 13b) and summer counterparts (Figures 13c and 13d). This suggests that winter temperature differences strongly decline, more so than summer temperature differences, which is consistent with Figures 11 and 12. The reductions in temperature difference are also enhanced under RCP8.5 (compared to RCP2.6), again consistent with Figures 11 and 12. However, the patterns are similar in the two scenarios, which is to some extent expected since the urban parameters used in the two scenarios are identical and constant over time. As an exception to the overall pattern across the domain, there are some regions displaying increasing summer trends such as the northeastern and southwestern US. These are regions where synergistic interactions between urban heat islands and the warming climate (i.e., the magnitude of urban-rural temperature difference is also increased when the background temperature increases) occur [*Li and Bou-Zeid*, 2013; *Li et al*., 2015] and

where city residents face higher health risks under a warming climate. This feature is also observed by Oleson [2012].

3.3. The Difference Between Urban Land Use Impacts and Traditionally Defined Urban Heat Islands

As mentioned in the introduction, the difference between urban temperature and some representative or averaged rural temperature is often called the "urban heat island" effect. The "urban land use impact" studied in the previous two sections compares the canopy air temperature of urban canyon to that of natural vegetation. The main difference between these two concepts is the definition of "rural temperature." In traditionally defined urban heat islands, the rural temperature often depends on the averaging procedure and as a result, the rural surface becomes conceptually abstract, whose properties such as albedo and roughness length also become difficult to interpret. However, given the wide use of such definition, we briefly discuss the difference between them in our simulation results. Figure 14 shows the comparison between these two concepts in summer (JJA) and winter (DJF). For Figures 14c and 14d, the rural temperature is defined as the area-average of nonurban (including cropland, pasture, natural and secondary vegetation) canopy air temperatures. It is clear that the urban heat islands calculated based on area-averaged rural temperatures (c, d) have similar spatial patterns as the urban land use impacts (a, b) in both summer and winter. The differences between the two have opposite signs in the two seasons: the urban land use impacts are larger in summer while the urban heat islands are larger in winter. Close inspection shows that this is mostly due to the difference between cropland and natural vegetation since cropland only affects the calculation of rural temperature in urban heat islands. In summer when croplands are generally hotter than natural vegetation [see *Malyshev et al*., 2015, Figure 4c], the urban heat islands are weaker since the averaged rural temperatures are higher than the natural vegetation temperature. On the other hand, in winter when croplands are cooler than natural vegetation [see *Malyshev et al*., 2015, Figure 5c], the urban heat islands are stronger due to the lower averaged rural temperature.

4. Conclusions

In the second part of the study we explore the urban land use impact by examining the difference between urban canyon and natural vegetation tiles in terms of daily averaged canyon air temperature over the CONUS using the newly developed LM3-UCM. We find that the temperature difference in summer is primarily affected by the contrast of evaporation and hence controlled by the precipitation amount. Despite significant variability, our simulations suggest that when the total summer precipitation amount is smaller than 400 mm, the temperature difference increases as the precipitation amount increases. This is due to the fact that increasing precipitation amount increases the water availability for evaporation in rural areas and thus reduces their canopy air temperatures. Water availability in urban areas also increases with precipitation, but it does not lead to the same increase of evaporation due to presence of impervious ground, and therefore urban canopy air temperatures are reduced less as the precipitation amount increases. Simulations also suggest that when the total summer precipitation amount is larger than 400 mm, the temperature difference no longer increases with increasing precipitation amount due to the limit of available energy for evaporation in rural areas (i.e., the evaporation rate in rural areas no longer increases as the precipitation amount increases). These results are broadly consistent with previous studies. The summertime temperature differences are also found to be significantly modulated by urban morphologies and properties. In winter, temperature differences are more controlled by the anthropogenic heating of buildings. These results show that the strong contributions of local background climate to urban heat islands shown in a recent study [*Zhao et al*., 2014] occur primarily in summer but not in winter. In addition, it is also found here that human activities such as urban morphologies and properties and building heating/cooling also play an important role in modulating urban-natural vegetation temperature differences. This has important implications for designing urban mitigation and adaption policies since it demonstrates that human activities can potentially control or alter heat stresses in cities by changing urban morphologies and properties, energy-use strategies, as well as human behaviors.

The responses of urban and natural vegetation temperatures to climate change are different, although they both increase due to increasing greenhouse gases. When averaged over the simulation domain, it is found that the trends of temperature differences are generally negative, suggesting that urban temperatures are increasing at a lower rate than rural temperatures. The trends are much stronger in the winter, which is

caused by reduced building heating rates under a warming climate. The comparison of temperature differences between 2081–2100 and 1981–2000 show that urban-natural vegetation temperature differences are reduced over most of the studied area in winter by the end of 21st century. However, there are some places displaying increasing trends such as the northeastern and southwestern US in summer, suggesting synergistic interactions with the warming climate (i.e., the increasing rate of urban temperatures is higher than that of rural temperatures).

Future improvements on the LM3-UCM model and input data are needed. In particular, neglecting the effect of air conditioning system might cause an underestimation of summer temperature differences and also affect their response to climate change. It is also shown here that the input data have an important effect on the simulated temperature differences and their spatial distribution. The unified global data set [*Jackson et al*., 2010] still suffers from coarse resolution in terms of morphological parameters and surface properties. The land-use transition data set [*Hurtt et al*., 2011] does not provide transitions among different urban tiles to represent for example a scenario that a low density urban area is developed into a high density urban area. The quality of these input data sets needs to be improved for global urban climate simulations.

Acknowledgments
Support from the NOAA (U.S. Department of Commerce) grant NA08OAR4320752 and the Carbon Mitigation Initiative at Princeton University, sponsored by BP, is acknowledged. The statements, findings, and conclusions are those of the authors and do not necessarily reflect the views of the NOAA, the U.S. Department of Commerce or BP. The code and simulation results can be obtained from the corresponding author.

References

Argueso, D., J. P. Evans, L. Fita, and K. J. Bormann (2014), Temperature response to future urbanization and climate change, *Clim. Dyn.*, *42*(7-8), 2183–2199.

Argueso, D., J. P. Evans, A. J. Pitman, and A. Di Luca (2015), Effects of city expansion on heat stress under climate change conditions, *Plos One*, *10*(2), e0117066.

Arnfield, A. J. (2003), Two decades of urban climate research: A review of turbulence, exchanges of energy and water, and the urban heat island, *Int. J. Climatol.*, *23*(1), 1–26, doi:10.1002/joc.859.

Budyko, M. I. (1963), *Evaporation Under Natural Conditions*, 130 pp., Israel Program for Sci. Transl. Off. of Tech. Serv., U.S. Dep. of Commer., Jerusalem.

Chen, F., et al. (2011), The integrated WRF/urban modelling system: Development, evaluation, and applications to urban environmental problems, *Int. J. Climatol.*, *31*(2), 273–288, doi:10.1002/joc.2158.

Conlon, K., A. Monaghan, M. Hayden, and O. Wilhelmi (2016), Potential impacts of future warming and land use changes on intra-urban heat exposure in Houston, *Plos One*, *11*(3), e0151226, Tex.

de Noblet-Ducoudre, N., et al. (2012), Determining robust impacts of land-use-induced land cover changes on surface climate over North America and Eurasia: Results from the first set of LUCID experiments, *J. Clim.*, *25*(9), 3261–3281.

Dunne, J. P., et al. (2012a), GFDL's ESM2 global coupled climate–carbon earth system models. Part II: Carbon system formulation and baseline simulation characteristics*, *J. Clim.*, *26*(7), 2247–2267, doi:10.1175/JCLI-D-12-00150.1.

Dunne, J. P., et al. (2012b), GFDL's ESM2 global coupled climate–carbon earth system models. Part I: Physical formulation and baseline simulation characteristics, *J. Clim.*, *25*(19), 6646–6665, doi:10.1175/JCLI-D-11-00560.1.

Fischer, E. M., K. W. Oleson, and D. M. Lawrence (2012), Contrasting urban and rural heat stress responses to climate change, *Geophys. Res. Lett.*, *39*, L03705, doi:10.1029/2011GL050576.

Georgescu, M. (2015), Challenges associated with adaptation to future urban expansion, *J. Clim.*, *28*(7), 2544–2563.

Georgescu, M., M. Moustaoui, A. Mahalov, and J. Dudhia (2013), Summer-time climate impacts of projected megapolitan expansion in Arizona, *Nat. Clim. Change*, *3*(1), 37–41.

Georgescu, M., P. E. Morefield, B. G. Bierwagen, and C. P. Weaver (2014), Urban adaptation can roll back warming of emerging megapolitan regions, *Proc. Natl. Acad. Sci. U. S. A.*, *111*(8), 2909–2914, doi:10.1073/pnas.1322280111.

Grimmond, C. S. B. (2007), Urbanization and global environmental change: Local effects of urban warming, *Geogr. J.*, *173*, 83–88, doi:10.1111/j.1475-4959.2007.232_3.x.

Grimmond, C. S. B., T. R. Oke, and H. A. Cleugh (1993), The role of "rural" in comparisons of observed suburban-rural flux differences, Exchange processes at the land surface for a range of space and time scales in *Proceedings of the Yokohama Symposium*, *IAHS Publ.*, *212*, 165–174.

Hurtt, G. C., et al. (2011), Harmonization of land-use scenarios for the period 1500–2100: 600 years of global gridded annual land-use transitions, wood harvest, and resulting secondary lands, *Clim. Change*, *109*(1-2), 117–161, doi:10.1007/s10584-011-0153-2.

Jackson, T. L., J. J. Feddema, K. W. Oleson, G. B. Bonan, and J. T. Bauerc (2010), Parameterization of urban characteristics for global climate modeling, *Ann. Assoc. Am. Geogr.*, *100*(4), 848–865.

Jacobson, M. Z., and J. E. Ten Hoeve (2012), Effects of urban surfaces and white roofs on global and regional climate, *J. Clim.*, *25*(3), 1028–1044, doi:10.1175/JCLI-D-11-00032.1.

Lawrence, D. M., et al. (2016), The Land Use Model Intercomparison Project (LUMIP): Rationale and experimental design, *Geosci. Model Dev. Discuss.*, (in review), doi:10.5194/gmd-2016-76.

Li, D., and E. Bou-Zeid (2013), Synergistic interactions between urban heat islands and heat waves: The impact in cities is larger than the sum of its parts, *J. Appl. Meteorol. Climatol.*, *52*(9), 2051–2064, doi:10.1175/JAMC-D-13-02.1.

Li, D., T. Sun, M. F. Liu, L. Yang, L. Wang, and Z. Q. Gao (2015), Contrasting responses of urban and rural surface energy budgets to heat waves explain synergies between urban heat islands and heat waves, *Environ. Res. Lett.*, *10*(5), 054009.

Malyshev, S., E. Shevliakova, R. J. Stouffer, and S. W. Pacala (2015), Contrasting local vs. regional effects of land-use-change induced heterogeneity on historical climate: Analysis with the GFDL Earth System Model, *J. Clim.*, *28*(13), 5448–5469, doi:10.1175/JCLI-D-14-00586.1.

McCarthy, M. P., M. J. Best, and R. A. Betts (2010), Climate change in cities due to global warming and urban effects, *Geophys. Res. Lett.*, *37*, L09705, doi:10.1029/2010GL042845.

Milly, P. C. D., S. L. Malyshev, E. Shevliakova, K. A. Dunne, K. L. Findell, T. Gleeson, Z. Liang, P. Phillipps, R. J. Stouffer, and S. Swenson (2014), An enhanced model of land water and energy for global hydrologic and earth-system studies, *J. Hydrometeorol.*, *15*(5), 1739–1761, doi:10.1175/Jhm-D-13-0162.1.

Oke, T. R. (1982), The energetic basis of the urban heat-island, *Q. J. R. Meteorol. Soc.*, *108*(455), 1–24, doi:10.1002/qj.49710845502.
Oke, T. R. (2006), Towards better scientific communication in urban climate, *Theor. Appl. Climatol.*, *84*(1-3), 179–190, doi:10.1007/s00704-005-0153-0.
Oleson, K. W. (2012), Contrasts between urban and rural climate in CCSM4 CMIP5 climate change scenarios, *J. Clim.*, *25*(5), 1390–1412, doi:10.1175/JCLI-D-11-00098.1.
Oleson, K. W., G. B. Bonan, J. Feddema, and T. Jackson (2011), An examination of urban heat island characteristics in a global climate model, *Int. J. Climatol.*, *31*(12), 1848–1865, doi:10.1002/joc.2201.
Pitman, A. J., et al. (2009), Uncertainties in climate responses to past land cover change: First results from the LUCID intercomparison study, *Geophys. Res. Lett.*, *36*, L14814, doi:10.1029/2009GL039076.
Shevliakova, E., S. W. Pacala, S. Malyshev, G. C. Hurtt, P. C. D. Milly, J. P. Caspersen, L. T. Sentman, J. P. Fisk, C. Wirth, and C. Crevoisier (2009), Carbon cycling under 300 years of land use change: Importance of the secondary vegetation sink, *Global Biogeochem. Cycles*, *23*, GB2022, doi:10.1029/2007GB003176.
Shevliakova, E., R. J. Stouffer, S. Malyshev, J. P. Krasting, G. C. Hurtt, and S. W. Pacala (2013), Historical warming reduced due to enhanced land carbon uptake, Proc. *Natl. Acad. Sci. U. S. A.*, *110*(42), 16,730–16,735, doi:10.1073/pnas.1314047110.
Stewart, I. D. (2011), A systematic review and scientific critique of methodology in modern urban heat island literature, *Int. J. Climatol.*, *31*(2), 200–217, doi:10.1002/joc.2141.
Zhao, L., X. Lee, R. B. Smith, and K. Oleson (2014), Strong contributions of local background climate to urban heat islands, *Nature*, *511*(7508), 216–219, doi:10.1038/nature13462.
Zhou, D. C., S. Q. Zhao, L. X. Zhang, G. Sun, and Y. Q. Liu (2015), The footprint of urban heat island effect in China, *Sci Rep.*, *5*, 11160, doi:10.1038/srep11160.